Estimation of the Vibrational Contribution to the Entropy Change Associated with the Low- to High-Spin Transition in $Fe(phen)_2(NCS)_2$ Complexes: Results Obtained by IR and Raman Spectroscopy and DFT Calculations

G. Brehm, M. Reiher,* and S. Schneider*

Institut für Physikalische und Theoretische Chemie, Universität Erlangen-Nürnberg, Egerlandstrasse 3, D-91058 Erlangen, Germany

Received: July 23, 2002; In Final Form: October 2, 2002

IR and Raman (λ_{ex} = 785 and 1064 nm) spectra of $Fe(phen)_2(NCS)_2$ were recorded at T = 298 and 100 K, and the observed vibrations were assigned by comparison with the results obtained by DFT/BP86 calculations. The latter resulted, in accordance with crystal data, in an equilibrium geometry with C_2 symmetry for the low-spin state. In the high-spin state, two closely lying extrema were found on the BP86 energy hypersurface: a saddle point (C_2 symmetry, one imaginary vibrational frequency) and, ca. 9.6 kJ/mol lower in energy, a minimum with C_1 symmetry. The differences in the geometrical parameters of the low-spin and high-spin states are in good agreement with the changes observed experimentally by X-ray crystallography. The calculated wavenumbers of the (NCS) vibration differed from the experimentally determined ones by more than 50 cm^{-1}. Since it could be shown that anharmonicity is not the only cause for this discrepancy, two pyridins at optimized distances were included to model the interaction in the crystalline state. We find a correct wavenumber shift of this solid-state model versus the isolated molecule, corroborating the prominent role of intermolecular interactions, which are considered to be responsible for the sharp transition from the low-spin to the high-spin state. The partition function was calculated for both spin states by considering all calculated vibrational wavenumbers. The vibration-related entropy change connected with the low- to high-spin transition is determined via well-known thermodynamic relations. For the title compound, we found $\Delta S_{vib} \approx 19.5$ J/(mol K), or approximately 40% of the experimentally determined total entropy change of 49 J/(mol K).

1. Introduction

Since its discovery some 70 years ago,[1,2] the phenomenon of a thermally induced transition from a low-spin (LS) state predominant at low temperatures to a high-spin (HS) state at higher temperatures, usually termed as "thermal spin crossover", has been extensively studied[3−17] by a multitude of experimental techniques. In accordance with the fact that the majority of spin crossover complexes contained Fe(II), ^{57}Fe Mössbauer spectroscopy[6] was preferentially applied to investigate the effect of temperature, pressure, concentration, phase, et cetera on this phenomenon. In 1974, Sorai and Seki[7] concluded from measurements of the molar heat, $c_p(T)$, that the increase in molar entropy connected with the LS-to-HS transition must be the essential driving force. As has already been pointed out by these authors, about 30% of the total change of $\Delta S \approx 50$ J/(mol K) originates from the electronic contribution:

$$\Delta S_{el} = R[\ln(2S+1)_{HS} - \ln(2S+1)_{LS}] = R\ln(2S+1)_{HS} \approx 13.4 \text{ J/(mol K)} \quad (1)$$

The remaining 70% are considered to be vibrational in nature because of the reduction of intramolecular vibrational frequencies. Therefore, the largest contribution is expected from the low-frequency modes related to the relative movement of the central metal and the nitrogen atoms that mediate the binding of the ligands.

To verify the above-described conclusions by Sorai and Seki, Bousseksou et al.[9] performed Raman experiments on $Fe(phen)_2(NCS)_2$ at 300 and 100 K to obtain the frequency shifts associated with the high−low-spin transition. Rather than making the attempt to calculate the partition functions in both spin states, they determined an average frequency shift from the bands observed in the range below 500 and 600 cm^{-1}, respectively, and assumed this value to be representative of all 15 distortion modes of an idealized FeN_6 octahedron. According to Bousseksou et al.,[9] the outcome of their first tentative approach "seems reasonable despite the severe limitations of their procedure and illustrates the utility of Raman spectroscopy to assess the vibrational contribution to the entropy change associated with spin crossover".

In this contribution, we present new IR and Raman spectra recorded at high and low temperature, respectively, thereby allowing us to establish a more complete set of experimental frequencies, especially in the low wavenumber region. In addition, we use these to validate the results of DFT calculations. On the basis of this first complete set of calculated normal-mode frequencies, the change in entropy can be calculated more reliably.

2. Materials and Methods

2.1. Materials. $Fe(phen)_2(NCS)_2$ was a gift from Dr. Franz Renz (Mainz, Germany). It was prepared according to the procedure described by Madeja[18] by extracting $[Fe(phen)_3](SCN)_2$ in a Soxhlet with dry acetone.

* To whom correspondence should be addressed. E-mail: schneider@chemie.uni-erlangen.de. Fax: (++49)9131-8528307. E-mail: Markus.Reiher@chemie.uni-erlangen.de.

10.1021/jp026586o CCC: $22.00
Published on Web 11/21/2002

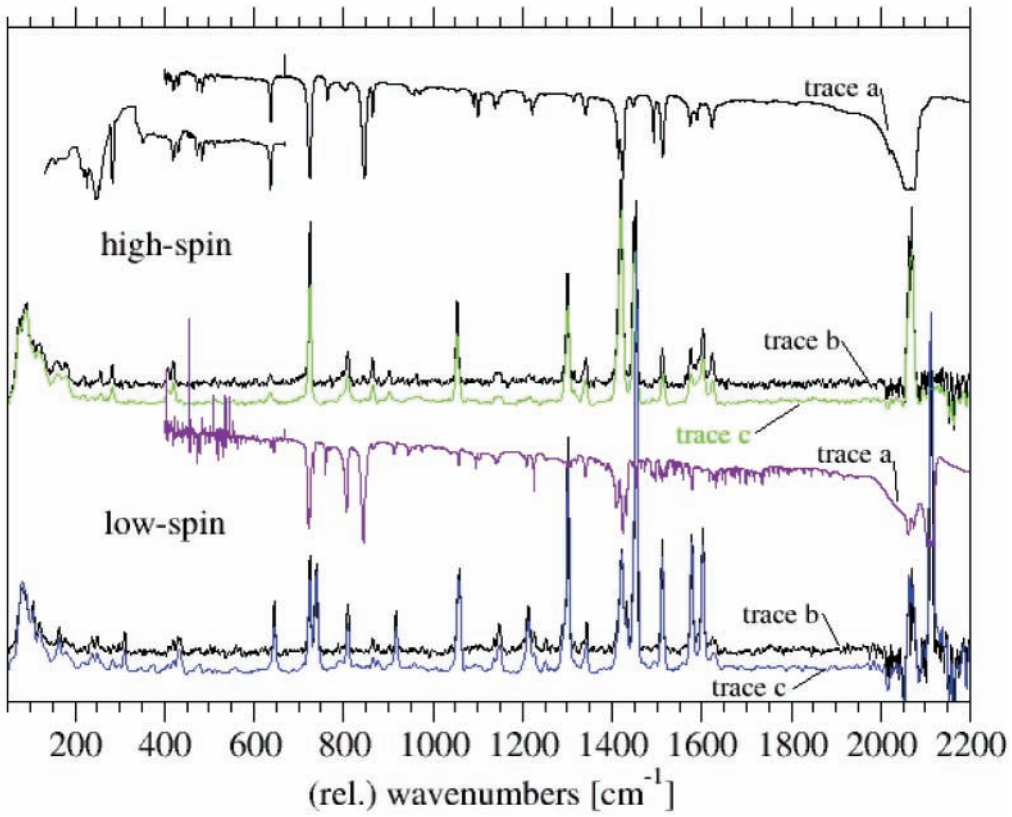

Figure 1. IR and Raman (λ_{ex} = 1064 nm) spectra of $Fe(phen)_2(NCS)_2$ recorded at 300 K (high-spin complex) and 100 K (low-spin complex). Spectral resolutions are (a) 2 cm^{-1}, FT-IR; (b) 1 cm^{-1}, Raman; and (c) 4 cm^{-1}, Raman.

The microcrystalline sample powder was diluted in CsI (FIR) and KBr (MIR, Raman), respectively, and formed into a pellet. The major reason for this procedure is that the application of neat crystalline material resulted in immediate destruction when the probing Raman laser (785 nm) was focused onto the sample. For FT-NIR Raman measurements, the neat sample powder was used.

2.2. IR and Raman Spectroscopy. IR spectra of pellets with 5 mg of sample/200 mg of matrix were recorded on a Bruker Equinox 55 spectrometer (resolution 2 cm^{-1} in FIR and 1 cm^{-1} in MIR).

Raman spectra were excited at 785 nm using a home-built Ti/sapphire laser pumped by an Ar^+ laser (Coherent, Innova 90-6). After dispersion in a double-grating spectrograph (Spex, model 1402), the Raman scattered light was detected by a liquid nitrogen-cooled CCD camera (ISA, model Spectrum One) with a spectral resolution of 2 cm^{-1}. The employed concentration was about 20 mg of sample/200 mg of KBr matrix.

Raman spectra with 1064-nm excitation were recorded with a Bruker RFS100 FT-Raman spectrometer (I = 200 mW, $\phi \approx$ 1 mm). For recording spectra at low temperature, the sample pellet was mounted to the coldfinger of a closed-cycle refrigerator (CTI Cryogenics, model CCS-150) employing KBr (IR) and quartz windows (Raman) in the evacuated sample chamber.

2.3. Quantum Chemical Methodology. All calculations were performed with the density functional programs provided by the Turbomole 5.1 suite.[19] The Becke−Perdew functional (BP86[20,21]) was selected because it is known to yield surprisingly good structural parameters and normal-mode frequencies.[26,28] In combination with these BP86 calculations, the resolution of the identity (RI) technique[22,23] was employed.

All reported results are obtained from fully optimized all-electron Kohn−Sham calculations in which the convergence thresholds were carefully adjusted for both the Kohn−Sham orbitals and the gradients using Ahlrichs' TZVP basis featuring a valence triple-ζ basis set with polarization functions on all atoms.[24]

For the vibrational analyses, the second derivatives of the total electronic energy were calculated as numerical first derivatives of analytic energy gradients,[25,26] which are provided by Turbomole. The vibrational contribution to the total entropy was computed within the harmonic approximation of the force field using the analytical results for the partition function of a harmonic oscillator.[26]

3. Results

3.1. IR and Raman Spectra. The IR and Raman spectra were recorded at 300 and 100 K (Figure 1). Since the transition temperature of $Fe(phen)_2(NCS)_2$ is known to be around T_c = 176 K,[7] the spectra characterize the high-spin (300 K) and low-spin complexes (100 K) well. Whereas in previous work[9] the lowest identified Raman vibrations were around 180 cm^{-1}, we could record spectra down to 60 cm^{-1} (Raman) and 150 cm^{-1} (IR). Because the CH stretching vibrations do not significantly contribute to the partition function, the spectral region above 2500 cm^{-1} is cut off. In Table 1, the experimentally determined wavenumbers are summarized for comparison with the corresponding calculated ones.

According to the crystal structure,[10] $Fe(phen)_2(NCS)_2$ exhibits C_2 symmetry. This implies that all normal modes can give rise to bands in both the IR and the Raman spectra. An inspection of Figure 1 and Table 1 shows that for many bands this double occurrence is actually observed.

As has been discussed earlier,[3,15] in the FIR region (100−500 cm^{-1}), significant shifts of the ligand-central Fe(II) stretching vibrations are expected. One reason is that upon transition

TABLE 1: Comparison of Experimental ($\tilde{\nu}_{exp}$) and Calculated ($\tilde{\nu}_{calc}$) Normal Mode Wavenumbers in cm^{-1} for the Low-Spin and High-Spin $Fe(phen)_2(NCS)_2$ Complex Observed in Raman (λ_{ex} = 785 and 1064 nm) and IR Spectra[a]

low-spin complex				high−spin complex			ligand	low-spin complex				high−spin complex			ligand
mode number	$\tilde{\nu}_{calcd}$	$\tilde{\nu}_{exptl}$ Raman	$\tilde{\nu}_{exptl}$ IR	$\tilde{\nu}_{calcd}$	$\tilde{\nu}_{exptl}$ Raman	$\tilde{\nu}_{exptl}$ IR	$\tilde{\nu}_{calcd}$ assigment	mode number	$\tilde{\nu}_{calcd}$	$\tilde{\nu}_{exptl}$ Raman	$\tilde{\nu}_{exptl}$ IR	$\tilde{\nu}_{calcd}$	$\tilde{\nu}_{exptl}$ Raman	$\tilde{\nu}_{exptl}$ IR	$\tilde{\nu}_{calcd}$ assigment
1	13			21				67	805	809	805/808	812	810	805	ωC−H
2	15			26				68	844	842		853	827		845
3	20			29				69	848		845	853	847	847	ring deform.
4	21			31				70	867	865	865	855			+
5	27			33				71	871	878		857	864	865	NCS
6	41			37				72	885			882			868
7	42			38				73	885			883			ring deform.
8	78			67				74	899			914	902	902	914
9	83	106		79	75			75	901			915			913
10	118	120		96	89			76	915		913	920			τC−H
11	154	133		99	92		99	77	915	917	916	922			
12	163	161		102			102	78	924			927			924
13	173			120	118			79	925			930			τC−H
14	178	176		135	127			80	931			941		852	936
15	182			138				81	931			941		856	τC−H
16	189	190		154	154	155		82	947		945	950		970	939
17	195			160	160			83	947		949	956		979	τC−H
18	216	212		163	174			84	1023	958/975		1025			1024
19	219			185	179			85	1025	1038		1027		1033	δNCC
20	229	233		194				86	1049	1054		1048	1054	1051	1031
21	250	246		198		222		87	1050	1048 s		1048			νC−C
22	254			227	217	227	223	88	1078		1058	1077			1063
23	274			230	(237)		227	89	1080			1077			δC−H νC−C
24	281	280		244	(243)		234	90	1084		1096	1082		1091	1083
25	291	293		248		249		91	1094	1102/1105		1087		1101	δC−H
26	307	304		259	255			92	1134			1131			1127
27	365	360		277	279			93	1135	1137	1138	1131			δC−H
28	375	368		282	283	284		94	1141		1144	1139	1139	1138	1140
29	377		390	288				95	1141	1148		1141	1144	1143	δC−H
30	407	399		392			383	96	1186			1187	1149		1188
31	413	411		399	399			97	1193		1200	1193	1191		δC−H
32	432			413	412		402	98	1210		1209	1212	1214	1207	1212
33	434	433		416	419	418		99	1210			1212			1209
34	439			424				100	1217	1213		1217		1222	νC−C δC−H
35	443			429		431		101	1217	1226	1226	1218	1228		
36	446			462			δNCS	102	1237	1252		1248	1246		1260
37	449			464				103	1238	1290		1249			νC−C δC−H
38	468	467		469			453	104	1308	1301	1301	1312		1300	1296
39	469	477	475	470			out-of-plane CCN +	105	1309		1307	1314	1315	1314	νC−N
40	489		479	473	473	473	ring deform.	106	1327		1321	1326			1320
41	491			474			δNCS	107	1328			1327			νC−N νC−C
42	494	493		478			489	108	1331		1340	1333	1336		1343
43	498	500		482	484		462	109	1332	1343	1342	1333	1341	1341	νC−N
44	505			490			out-of-plane CCN	110	1394			1397	1388		1372
45	505			493	499		δNCS	111	1395			1398			νC−C
46	520	521		505			507	112	1410		1409	1400			
47	526		558	505	513	512	ring deform.	113	1410	1415	1412	1401			1401
48	556	556		550			546	114	1413	1421	1424	1408			1410
49	557			552			540	115	1413			1408	1415	1414	νC−C νC−H
50	571			553			ring deform.	116	1442	1433	1431	1427	1420	1425	1435
51	576	592		555		(559)	+ out-of-plane CCN	117	1442	1454	1436	1433	1449	1448	νC−C
52	633			622			612	118	1478		1455	1483	1474		1486
53	638	640		626	636	637		119	1480			1484			νC−C νC−N
54	649		645	660			674	120	1491			1486			1488
55	652			663				121	1497			1495	1495	1493	νC−C νC−N
56	669			690			706	122	1546	1512		1541	1512	1512	1532
57	675			692				123	1546			1543			νC−C νC−N
58	718		720	705			694	124	1547			1556			1579
59	720		722	714			ring deform.	125	1552			1559			νC−C νC−N
60	725	725	724	719		722	722	126	1572			1581	1575	1574	1593
61	736		734	720	725	725	ring deform.	127	1572	1578	1576	1582	1590	1590	νC−C νC−N
62	741	740 s		746			741	128	1609	1603		1605	1602	1603	1608
63	742			749	763		ωC−H	129	1610	1627	1631	1605	1623	1623	νC−C
64	769		760	780	770		778	130	2061	2107	2107	2029	2062	2062	NCS
65	771			781	788		ωC−H	131	2070	2110	2110	2040	2072	2072	NCS
66	805		800	810	797	797	811								

[a] Calculated modes of the high-spin complex are also compared with the calculated modes of the free ligand−1,10-phenanthroline−and the NCS vibrations.

to the high-spin state (in an ideal octahedral environment) two electrons are promoted from a bonding t_{2g} orbital into an antibonding e_g orbital, thus weakening the metal-to-ligand binding. However, the extent of $d_\pi-p_\pi$ back-bonding to the ligand is also reduced with the effect that the frequency of the (NCS) stretching vibration is lower in the high-spin state than in the low-spin state (2072 versus 2110 cm^{-1}).

Whereas the assignment of the latter vibration is quite unique, the identification of the other corresponding pairs of vibrational bands in the high- and low-spin states, respectively, is difficult and is therefore performed by comparison with the results of the quantum chemical calculations (see below). In any case, it is noteworthy that for wavenumbers above 1000 cm^{-1} the location of several of the stronger bands is conserved within experimental accuracy. This can be rationalized by the assumption that those vibrations of the phenanthroline ligand, which do not involve major movement of the coordinating nitrogens, are not influenced by the LS-to-HS transition of the central metal atom. Attempts to record (resonance-enhanced) Raman spectra of $Fe(phen)_2(NCS)_2$ in solution have failed so far because of solubility reasons.

3.2. Quantum Chemical Calculations. For DFT calculations of compounds such as $Fe(phen)_2(NCS)_2$, the functional must be optimized to get a physically meaningful low-spin−high-spin energy splitting[30,31] (the results are reported elsewhere[27]). The determination of ΔH for the low-spin−high-spin transition requires the very accurate calculation of an "excited-state" energy and is therefore, in general, much more difficult than the determination of the corresponding sets of normal-mode frequencies. For the latter, only the calculation of the relative changes of the involved potential energy surfaces is necessary. This implies that even at a lower level of accuracy for excitation energies a functional such as BP86 yields fairly good values for equilibrium geometry and vibrational frequencies.

The BP86/RI/TZVP calculations predict as the lowest singlet energy conformation one (Figure 2a) that resembles closely the published X-ray structure of $Fe(phen)_2(NCS)_2$. The complex exhibits C_2 symmetry with the two NCS ligands in a cisoid position. An isomer with the two NCS ligands in a transoid position (Figure 2b) is calculated to be higher in energy by about 54.1 kJ/mol. Selected geometrical parameters are compared in Table 2. For both geometries, the calculations yield a complete set of normal-mode frequencies (Table 1).

The optimized high-spin (quintet) structure with C_2 symmetry represents a first-order saddle point on the potential energy surface (PES) since it possesses one imaginary frequency. (Please note that we ensured that this is not an artifact of the C_2-symmetric electronic wave function due to the wrong occupation of a- and b-symmetric orbitals.) Since we calculated the numerical frequencies seminumerically from the first derivatives of the analytic energy gradients,[25,26] the modes at very small wavenumbers are subject to numerical inaccuracies. Numerical inaccuracies can usually be diminished by increasing the accuracy of the wave function. We therefore improved the optimization and converged the norm of the energy gradient to 10^{-5} and the electronic energy to 10^{-9} on a finer numerical integration grid for the DFT method. However, even these sharp iteration thresholds did not yield an improved vibrational spectrum, and the imaginary frequency did not vanish. This is considered to be good evidence that, when calculated with the BP86 density functional, the high-spin complex in C_2 symmetry represents a true saddle point. Optimization of the structure in C_1 symmetry resulted in a decrease in the electronic energy by ca. 9.6 kJ/mol, and a subsequent vibrational analysis confirmed

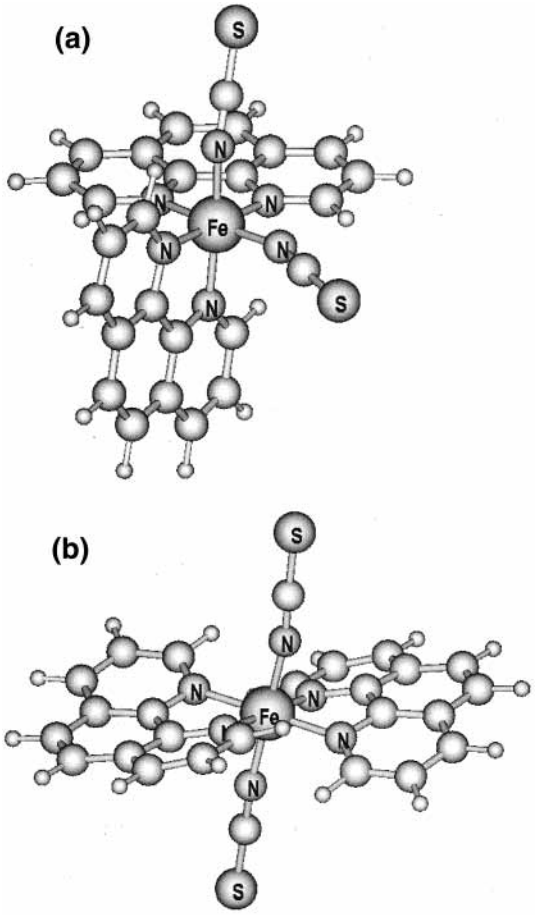

Figure 2. Calculated structures of $Fe(phen)_2(NCS)_2$ in the low-spin state. (a) Minimum-energy conformation (cisoid); (b) transoid isomer ($\Delta E \approx 54.1$ kJ/mol).

that the obtained C_1 structure is a minimum structure on the PES. Our present methodology is not able to resolve this puzzle of symmetry reduction because the preference of an unsymmetric HS state over a C_2-symmetric one depends on the density functional chosen.[27] The vibrational spectrum of the slightly distorted, C_1-symmetric high-spin structure (Figure 3) is very similar to the spectrum for the C_2 high-spin structure (deviations amount to about 2 cm^{-1} per mode, which is small compared to the accuracy of the method).

Accordingly, in Figure 4, the geometries of $Fe(phen)_2(NCS)_2$ in both the C_1 high- and the C_2 low-spin states are compared. The already mentioned increase in the length of the metal-to-ligand bonds is reproduced by the calculations (see also Table 2). The increase in the length of bonds to the phenanthroline nitrogens is, however, overestimated by about 30%, whereas the increase in the length of bonds to the (NCS) ligands is underestimated by about 30% (versus the crystal structure). Similarly, the bond lengths in the (NCS) ligands are changed in correspondence with the mentioned frequency changes of the (NCS) stretching vibrations. The reduction in the CS bond length is properly predicted, but the increase in the NC bond length is underestimated. Because there is also a significant difference between calculated and experimentally determined bond distances in the low-spin-state structure, one can conclude that the complex geometries found in the crystalline state are most likely influenced by packing effects.

The data presented additionally in Table 2 also show that the deviation from C_2 symmetry has only a very small effect on the relevant bond distances and bond angles in the high-

TABLE 2: Comparison of Selected Geometrical Parameters of Transoid Fe(phen)$_2$ (NCS)$_2$ in the Low-Spin State (C_2 Symmetry) and the Cisoid High-Spin State (C_1 Symmetry) and the Cisoid Ground State[a]

parameter	LS C_2	exptl	HS C_1	exptl	Δ(calcd)	Δ(exptl)	LS(calcd) transoid
d(Fe−N$_i$)	193.2	195.8	199.7	205.7	6.5	9.9	192.3
d(N$_i$−C$_i$)	119.3	114.0	119.5	115.8	0.2	1.8	119.0
d(C$_i$−S$_i$)	162.7	163.2	162.2	162.8	−0.5	−0.4	163.1
d(Fe−N(phen)1)	195.3	201.4	219.9	219.9	24.6	18.5	198.3
d(Fe−N(phen)1′)	196.6	200.5	228.3	221.3	31.7	20.8	197.6
d(Fe−N(phen)2)	195.3	201.4	220.0	219.9	24.7	18.5	197.6
d(Fe−N(phen)2′)	196.6	200.5	228.5	221.3	31.9	20.8	198.3
α(N(phen)1FeN(phen)1′)	82.8	81.8	74.1	76.1	−8.7	−5.7	81.6
α(N(phen)2FeN(phen)2′)	82.8	81.8	74.0	76.1	−8.0	−5.7	81.6
α(FeN$_1$C$_1$)	156.8	165.6	168.0	167.0	11.2	1.4	172.0
α(N$_1$C$_1$S$_1$)	177.4	179.5	179.3	179.4	1.9	−0.1	178.9
α(FeN$_2$C$_2$)	156.8	165.6	168.1	167.0	11.3	1.4	172.0
α(N$_2$C$_2$S$_2$)	177.4	179.5	179.2	179.4	1.8	−0.1	178.9

[a] Included are experimental data taken from ref 10. (Distances in pm, angles in deg; Δ refers to the change upon the LS−HS transition.)

Figure 3. Model to reflect interactions in the unit cell.

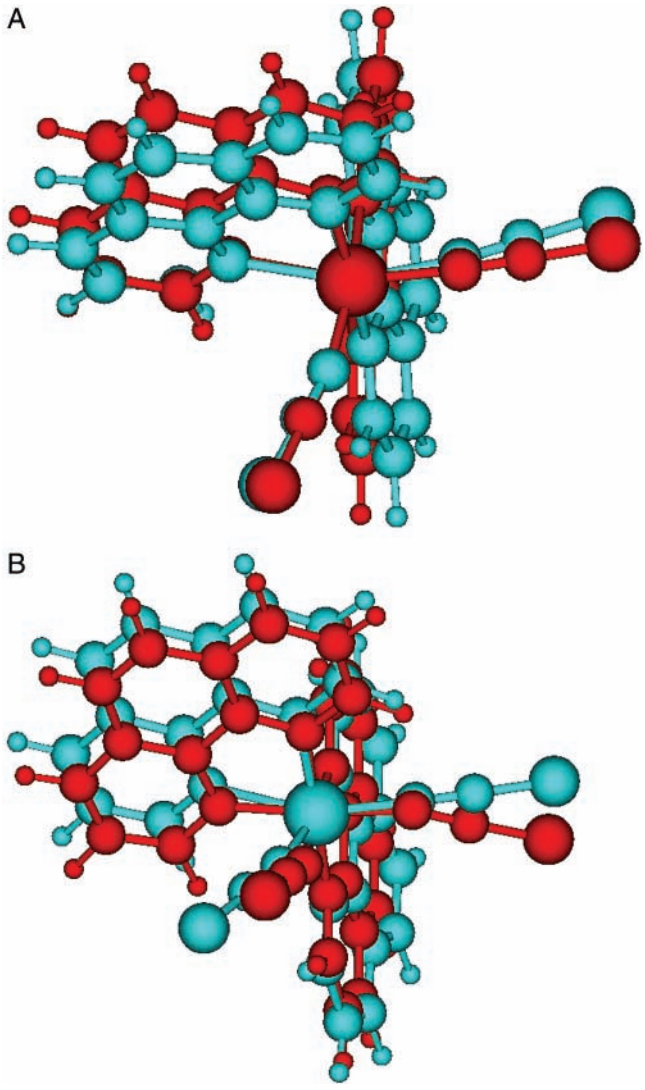

Figure 4. (a) Superimposed high-spin (quintet) structures obtained for C_2 and C_1 symmetry. Blue represents the C_1 high-spin structure, and red , the C_2 high-spin structure. (b) Superimposed C_2 low-spin and C_1 high-spin structures. Blue represents the C_1 high-spin structure, and red, the C_2 low-spin structure.

spin state. They are, in any case, much smaller than the differences between calculated and experimentally determined parameters.

For the sake of completeness, it should be mentioned that many of the structural parameters of the higher energetic transoid isomer are very similar to those of the cisoid isomer (Table 2).

An additional crucial test for the validity of the calculations is the correct prediction of the shift of the uniquely identified (NCS)$_2$ stretching vibrations. For the LS complex, both a symmetric and an antisymmetric stretching vibration are predicted at 2061 and 2070 cm^{-1}, respectively. In the Raman and IR spectra, a strong band is observed around 2110 cm^{-1}, accompanied by a shoulder around 2107 cm^{-1}. For the HS complex, the corresponding pair of bands is predicted at 2029 and 2040 cm^{-1}, whereas the experimental values are 2062 and 2072 cm^{-1}. In conclusion, experimental and calculated wavenumbers differ for this mode by about 50 cm^{-1}. Since the accuracy of frequencies obtained from harmonic BP86/RI/TZVP force fields is, however, known to be often better than 10 cm^{-1} for large Fe(II) and Ru(II) complexes,[28,29] we investigated two possible reasons for the observed deviation of up to 50 cm^{-1}: (i) the break down of the harmonic approximation for those normal modes, which mainly involve vibrations of the NCS groups and (ii) the neglect of the actual experimental situation in the condensed phase in the quantum chemical calculations of the isolated spin-crossover complexes.

The anharmonicity of the potential energy curve along a NCS normal mode could only be checked through the calculation of displacement structures along this NCS mode. For instance, expansion (or compression) of the C−N bonds by ca. 0.23 pm and of the C−S bonds by ca. 0.14 pm occurs in the perfectly harmonic region, whereas anharmonicity plays an increasing role for larger distortions. However, there currently exists no reliable computational technique for the estimation of the frequency shifts due to the anharmonicity of the PES for large molecules such as the complex under study. Whereas variational approaches for this purpose would be highly unfeasible, the perturbation theory approach fails because of the occurrence of Fermi resonances.

The validity of the isolated-molecule approach can be tested within our quantum chemical methodology only by the generation of a suitable model compound that contains essential features of the arrangement in the solid state. The crystal structure[10] shows that phenanthroline groups of neighboring molecules come as close as 336.7 pm (which is the intermolecular distance between a phenanthroline C atom and a NCS sulfur atom; note that the corresponding H−S distance is much smaller). Therefore, we generated a model structure with C_2 symmetry with two pyridine molecules (as models for the larger phenanthroline ligands) close to the sulfur atoms (Figure 2c). Upon structure optimization, the intermolecular distance between a pyridine C atom and the sulfur atom increases to 408.0 pm. The pyridine molecules thus affect the $Fe(phen)_2(NCS)_2$ to a lesser extent than the phenanthroline ligands in the solid state, where packing effects can cause smaller distances. Furthermore, our model does not take into account that the phenanthroline ligands in $Fe(phen)_2(NCS)_2$ would also interact with the next neighboring NCS ligands in the solid state.

The vibrational analysis of the described pyridine adduct model system generally yields a shift of the NCS modes to higher wavenumbers. For the low-spin complex, one finds 2098 and 2109 cm^{-1} for the corresponding symmetric and antisymmetric stretching vibrations, respectively. This indicates that a large fraction of the observed discrepancy between the experimental wavenumber of the crystalline material and the wavenumber calculated for the isolated molecule is indeed due to interactions present only in the crystal.

4. Discussion

4.1. Matching between Experimental and Calculated Spectra. The calculations predict 17 modes with frequencies below 200 cm^{-1} for the low-spin (LS) complex and 21 modes for the high-spin (HS) complex. In the Raman and IR spectra, six LS and nine HS bands, respectively, can be identified beyond doubt below 200 cm^{-1}. This shows that about one-half of the low-wavenumber modes that make a major contribution to the vibrational partition function are experimentally not accessible. An analysis of the corresponding normal-coordinate pictures (a representative selection is presented in Figure 5) proves that the modes with frequencies below 100 cm^{-1} comprise mainly out-of-plane motions of the phenanthroline ligand.

In the spectral range of $200 < \tilde{\nu}/cm^{-1} < 500$, the calculations predict 26 bands for the LS and 24 bands for the HS complex. These numbers contrast with 15 experimentally observed bands for the LS and 14 bands for the HS complex. Bousseksou et al.[9] argued that some of the weak bands, which appeared not only in the low-temperature but also in the high-temperature Raman spectrum, could originate from remainders of HS complexes and were therefore ignored in their evaluation of ΔS_{vib}. By comparison with the calculated results, it is obvious that such an assumption is most likely incorrect for many of these bands. In the theoretical spectra of the low-spin and high-spin complexes, about 10 modes are predicted in this region, with wavenumbers equal to about ±1 cm^{-1}. Among these are, for example, the modes with numbers 11/16 (154 cm^{-1}) 12/18 (163 cm^{-1}), 17/20 (195 cm^{-1}), 20/23 (229 cm^{-1}), 24/28 (281 cm^{-1}), 31/32 (413 cm^{-1}), 38,39/38,39 (468/469 cm^{-1}), and 40/44 (489 cm^{-1}) or 41/44 (491 cm^{-1}).

In this context, it is worthwhile to mention that the Raman and IR spectra of the isolated phenanthroline ligand exhibit also only a small number of bands below 500 cm^{-1}, namely, 6 in the IR and 11 in the Raman spectrum. The agreement between experimental and calculated wavenumbers is excellent,[32] thus providing additional information for the assignment of the phenanthroline-related low-wavenumber modes.

The statements about the number of calculated versus experimentally observed bands in the spectral regions of $\tilde{\nu} < 500\ cm^{-1}$ are similarly valid for the spectral ranges of $500 < \tilde{\nu}/cm^{-1} < 1000$ (40 calculated modes) and $1000 < \tilde{\nu}/cm^{-1} < 1650$ (about 45 calculated modes). Although the contribution of each individual normal mode to the partition function should be small because of an unfavorable Boltzmann factor for high-frequency modes, they could add a significant contribution to ΔS_{vib} provided that the wavenumbers change significantly upon the LS-to-HS transition. The experimental spectra, however, do not provide much evidence for such large shifts and are corroborated in this respect by the results of the calculations.

4.2. Assignment of Vibrational Bands. Our assignment of the experimentally observed modes to the calculated ones is presented in Table 1. In spectral regions where the density of bands is not too high, such a correlation is possible by just comparing the wavenumbers. In cases of sufficiently intense IR or Raman bands, the calculated intensities are taken into account as an additional criterion.

In previous work,[3,15−17] iron−ligand bond-stretching vibrations could be identified by means of isotope substitution. Accordingly, they should be found in the wavenumber range of 250−300 cm^{-1} for the high-spin isomers and in the range of 400−500 cm^{-1} for the low-spin isomer. Inspection of the normal-coordinate pictures reveals that in our compound serveral modes are found in the mentioned spectral region that exhibit a large movement of the iron atom relative to the position of the attached ensemble of ligands. Two examples are shown in Figure 5. In the pair of related modes, namely, number 25 (LS; 291 cm^{-1}) and 21 (HS; 282 cm^{-1}), the iron atom moves vertically in the chosen representation. In the second pair, namely, number 29 (LS; 377 cm^{-1}) and 28 (HS; 282 cm^{-1}), the iron atom moves, with the equivalent orientation of the ligands, horizontally. The generally adopted assumption of an increase in the stretching frequency of the metal-to-ligand bonds upon a HS−LS transition is verified. But a closer inspection of the normal-mode coordinates shows that the mixing pattern of local movements in the ligands is different in the HS and LS isomers. This can be rationalized with a simple picture. If the bond strength is increased concomitantly with the frequency of the localized metal-to-ligand stretching vibration, then this mode will preferentially couple with those local modes of the ligands whose frequency is also higher.

As mentioned above, one finds many coincidences in wavenumbers when comparing the theoretical spectra of the low-spin and high-spin complexes, respectively. The suggestion that this is indicative for normal modes that do not change the binding between central metal and ligand(s) is often falsified by the actual normal-coordinate pictures. One example is given

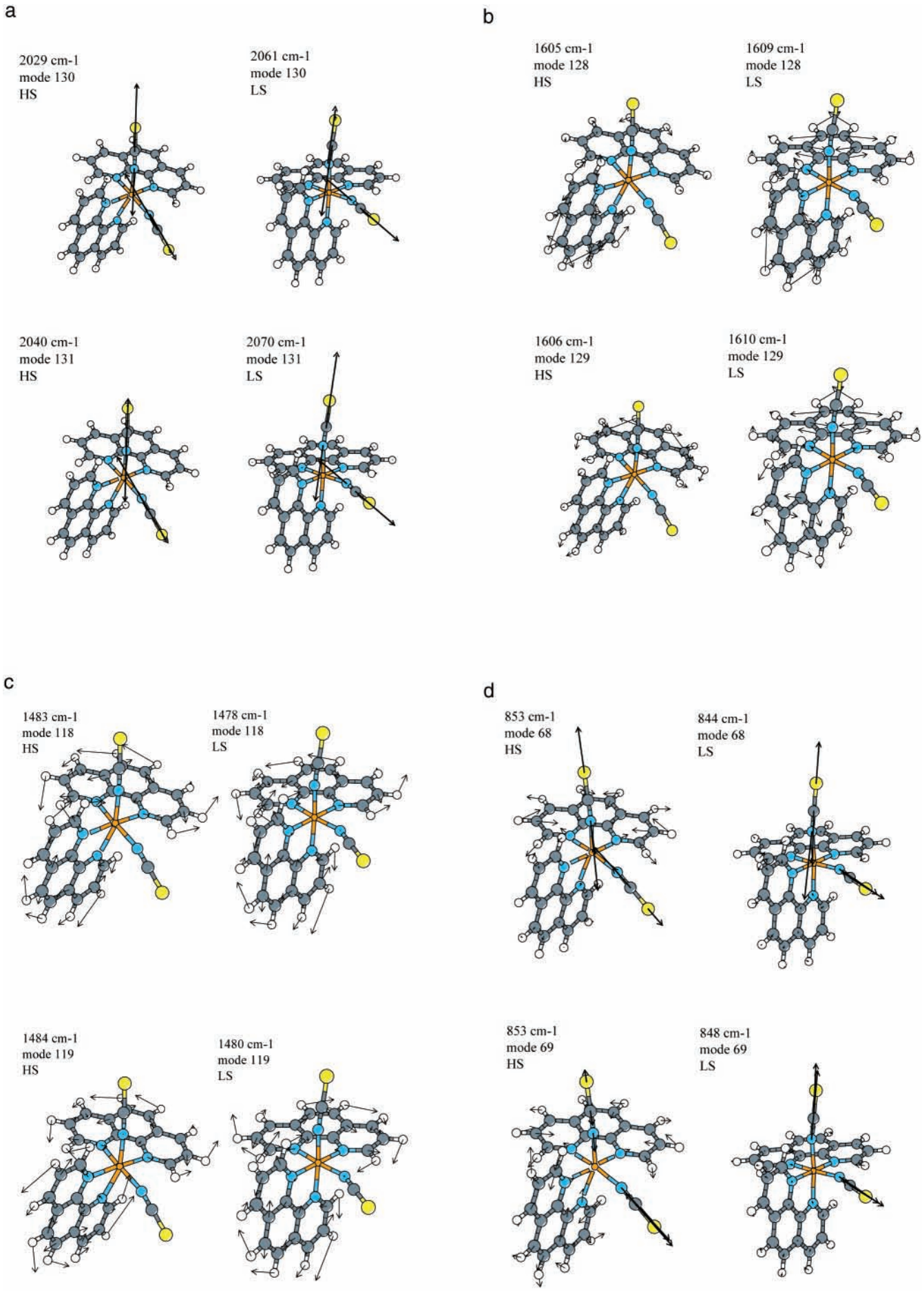
a
2029 cm-1
mode 130
HS
2061 cm-1
mode 130
LS
2040 cm-1
mode 131
HS
2070 cm-1
mode 131
LS
b
1605 cm-1
mode 128
HS
1609 cm-1
mode 128
LS
1606 cm-1
mode 129
HS
1610 cm-1
mode 129
LS
c
1483 cm-1
mode 118
HS
1478 cm-1
mode 118
LS
1484 cm-1
mode 119
HS
1480 cm-1
mode 119
LS
d
853 cm-1
mode 68
HS
844 cm-1
mode 68
LS
853 cm-1
mode 69
HS
848 cm-1
mode 69
LS

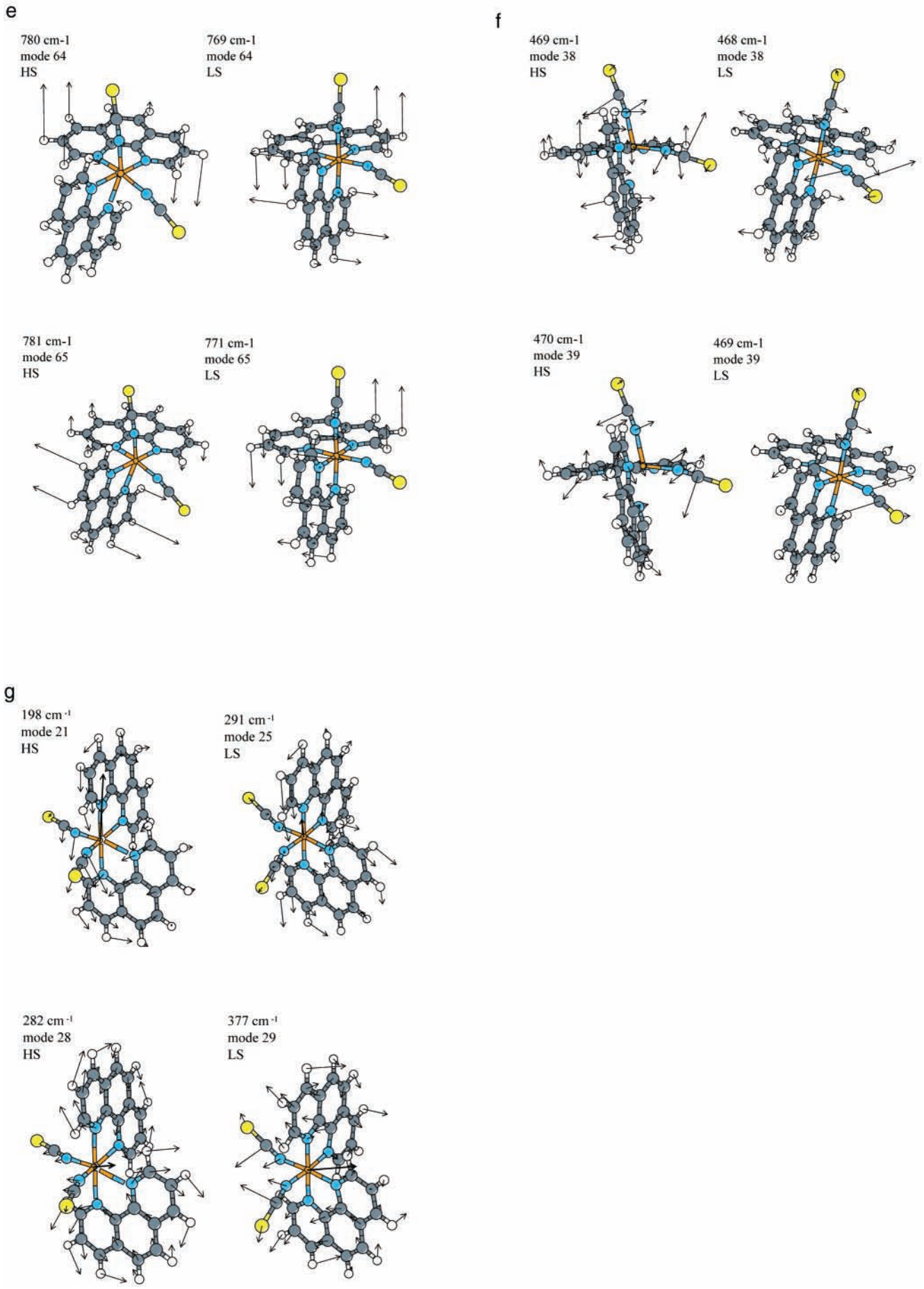

Figure 5. Selected normal coordinates calculated for low-spin (right side, a−g) and high-spin complexes (left side, a−g).

in Figure 5, where the displacement vectors of modes 38 and 39 are shown for comparison. Both modes comprise a large movement of the two NCS ligands, thereby changing the length of the two metal-to-nitrogen bonds and the angle in between. The contribution of the local modes of the two phenanthroline ligands is pronouncedly different in the low-spin and high-spin complexes.

The displacement vectors of modes 64 and 65, respectively, are essentially localized on the phenanthroline ligands with nearly no movement of the ligating nitrogen atoms or the atoms of the NCS groups. Nevertheless, the modified interaction between the phenanthroline moieties and the central metal leads to a significant shift of the corresponding wavenumbers in the low-spin versus high-spin complex.

Modes 68 and 69, respectively, can be characterized as stretching vibrations of the metal-to-ligand bonds involving mainly the NCS but also the phenathroline ligand. In contrast to the previously mentioned expectation, the wavenumbers of these modes are higher in the high-spin than in the low-spin complex. But for modes 70 and 71, in which the contribution of the phenathroline ligand dominates, the wavenumbers shift from 867/871 cm^{-1} (LS) to 855/857 cm^{-1} (HS).

It should be noted in passing that most of the bands observed around 900 cm^{-1} can be assigned, by comparison with the calculated normal coordinates, to hydrogen out-of-plane motions.

Those normal modes, which represent essentially hydrogen in-plane motions of the phenanthroline ligands, are found around 1480 cm^{-1}. As documented by modes 118 and 119, their wavenumbers are practically unchanged upon the LS-to-HS transition. The same conclusion is also valid for the modes involving the C═C double-bond stretching in the phenanthroline ligand (e.g., modes 128 and 129).

The already-discussed stretching mode of the NCS ligands is also visualized in Figure 5. The displacement vectors are indeed localized only on these ligands. Therefore, the change in wavenumber truly reflects the change in bond strength.

The examples given demonstrate that it is rather difficult, if not impossible, to make a generally valid statement about the frequency shifts correlated with the low-spin−high-spin transition of the central metal.

4.3. Calculation of the Entropy Change ΔS Associated with the LS-to-HS Transition. From direct caloric measurements, in the case of abrupt transitions, or from values derived via thermodynamic relationships in the case of progressive spin crossover, a large body of data concerning the entropy change associated with the LS-to-HS transition of Fe(II) complexes can be found in the literature.[7,12−14] The reported ΔS values range between 45 and 58 J/(mol K). This means that the above-mentioned value of $\Delta S = 49$ J/(mol K) for $Fe(phen)_2(NCS)_2$ lies close to the average value.

The total change in entropy ΔS connected with the LS-to-HS transition can be divided into an electronic contribution and contributions originating from vibrational and, in the gas phase, from rotational degrees of freedom:

$$\Delta S = \Delta S_{el} + \Delta S_{vib} + \Delta S_{rot} \qquad (2)$$

(Notice that in this model the translational contribution would be the same for both spin states and thus it need not be taken into account).

The electronic contribution is given by the spin-only value of the fivefold-degenerate high-spin wave function

$$\Delta S_{el} = R \ln(2S+1)_{HS} = R \ln(5) = 13.38 \text{ J/(mol K)}$$

TABLE 3: Estimates for the Different Contributions to the Total Entropy in the Various Electronic States of $Fe(phen)_2(NCS)_2$ and Their Changes upon the Low-Spin to High-Spin Transition[a]

	S_{el}	S_{rot}	σ	S_{vib}	S_{tot}	ΔS_{vib}	ΔS_{tot}	$T_c\Delta S_{tot}$
LS C_2	0	141.6	2	289.3	607.0	0.0	0.0	0.0
HS C_1	13.4	148.6	1	308.8	646.8	19.5	39.8	7.0

[a] Entropies are in J/(mol K), and energies are in kJ/mol at $T_c = 176$ K.

where we must assume that the electronically excited states are so much higher in energy that they cannot be excited thermally.

The entropy contribution of the rotational degrees of freedom to the spin crossover phenomenon can be estimated in the framework of a semiclassical model, which yields

$$S_{rot} = R(\ln(z_{rot}) + {}^3/_2)$$
$$\text{with } z_{rot} = (\sqrt{2}/\hbar)^3\sqrt{\pi}/\sigma(kT)^{3/2}(J_1 \cdot J_2 \cdot J_3)^{1/2} \qquad (3)$$

where σ is the symmetry number, which is 2 in the case of C_2 and 1 in the case of C_1 symmetry, and the J_i's are the moments of inertia.

If one inserts the structural data obtained by the calculations, one gets moments of inertia that are very similar in size. In the case of conservation of C_2 symmetry, the related change in entropy, ΔS_{rot}, could easily be neglected in the estimate of the total entropy change. If one adopts the prediction of the calculations, that is, symmetry reduction, then for a freely rotating molecule, ΔS_{rot} amounts to 7 J/(mol K), mainly as an effect of the change in symmetry number. In the crystalline state, free rotation is prohibited, but librations around the equilibrium configuration could occur. The contribution to ΔS should be much lower than the above estimate of $\Delta S_{rot} = 7$ J/(mol K). However, one should consider the contribution of the phonons. Since the crystal dimensions are reduced on the LS-to-HS transition, one can expect significant changes in the phonon frequencies. But on the basis of our present methodology, we cannot make a reasonable estimate of this contribution.

The vibrational contribution is calculated from the frequencies $\nu_i = c\tilde{\nu}_i$ in the harmonic approximation according to

$$S_{vib} = \sum_i \{h\nu_i/kT[\exp(h\nu_i/kT) - 1]^{-1} -$$
$$\ln[1 - \exp(-h\nu_i/kT)]\} \qquad (4)$$

If one applies the complete set of normal-mode wavenumbers produced for the low-spin state with C_2 symmetry and the corresponding set of normal modes calculated for the high-spin state with C_1 symmetry, then one gets an increase of 19.5 J/(mol K) in the vibration-related entropy (see Table 3). For comparison, please remember that the omission of a normal mode with $\tilde{\nu} \approx 10$ cm^{-1} would, at $T_c = 176$ K, correspond to a reduction in vibrational entropy of 29.1 J/(mol K). With respect to error analysis, it therefore seems worthwhile to analyze the contributions of modes in different spectral regions.

The first 10 normal modes, whose wavenumbers are calculated to be certainly below about 120 cm^{-1}, contribute to the molar entropy values of 188.1 J/(mol K) and 175.8 J/(mol K) for the low-spin and high-spin complexes, respectively (see Figure 6). This implies that these modes give rise to an entropy decrease upon the HS-to-LS transition of about 12.3 J/(mol K).

Modes 11 to 32, which roughly span the wavenumber region of $100 < \tilde{\nu}/cm^{-1} < 420$, contribute 82.9 and 113.7 J/(mol K), respectively, to the total entropy. This implies that by taking

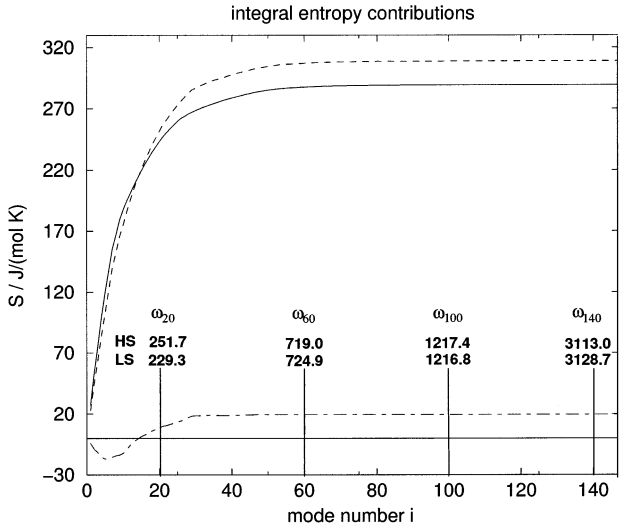

Figure 6. Vibrational entropy of the high-spin (HS, - - -) and the low-spin (LS, —) complexes, with the normal modes included up to the *i*th mode in the calculations, compare eq 4. Additionally, the entropy change $S_i(\mathrm{HS}) - S_i(\mathrm{LS})$ is shown (— - —).

into consideration only the lowest 32 vibrational modes one gets an estimate for ΔS_{vib} that is essentially equal to the final value. A detailed analysis confirms that the remaining higher-wavenumber normal modes contribute, as expected, very little to the entropy change, namely, (19.2−18.4) J/(mol K) = 0.8 J/(mol K).

By adding the estimates for ΔS_{el} and ΔS_{vib}, one gets a total entropy change at $T_c = 176$ K of 32.9 J/(mol K) if a structurally relaxed high-spin state with C_1 symmetry is assumed. The entropy change due to rotation should be less than 7 J/(mol K). The corresponding contribution to ΔG (HS−LS), namely, $T_c\Delta S_{\mathrm{vib}}$, amounts to about 3.4 kJ/mol and is therefore similar in size to $\Delta H(T_c)$, as required for the vanishing difference of the free enthalpies at the spin-crossover temperature (i.e., $\Delta G(T_c) = 0$).

It was mentioned above that Bousseksou et al.[9] rather than summing over all vibrational modes used a low-frequency approximation yielding

$$\Delta S_{\mathrm{vib}} = pR \ln(\tilde{\nu}_{\mathrm{LS}}/\tilde{\nu}_{\mathrm{HS}}) \qquad (5)$$

where $\tilde{\nu}_{\mathrm{LS}}$ and $\tilde{\nu}_{\mathrm{HS}}$ represent an average wavenumber in both states and p, the number of oscillators to be considered. Inserting a frequency ratio $\tilde{\nu}_{\mathrm{LS}}/\tilde{\nu}_{\mathrm{HS}}$ of 1.3, respectively, $\tilde{\nu}_{\mathrm{HS}}/\tilde{\nu}_{\mathrm{LS}} = 0.77$ for modes below 600 cm^{-1} and $p = 15$ modes, Bousseksou et al. obtained $\Delta S_{\mathrm{vib}} \approx 20 \pm 1$ J/(mol K), in astonishing agreement with our result. This number leaves a difference of about 16 J/(mol K) to the estimation by Sorai and Seki[7] and was proposed by Bousseksou et al. to originate from other low-frequency modes that were not included. Our calculations show that the latter conclusion is most likely not justified. In Figure 7, the ratio of the wavenumbers of each pair of calculated normal modes, $R_i = \tilde{\nu}_{i(\mathrm{LS})}/\tilde{\nu}_{i(\mathrm{HS})}$, is shown. For the lowest-wavenumber modes, this ratio is larger than 1, and for modes 5 to 36, it is consistently smaller than 1. For the higher-number modes, the ratio fluctuates around 1. As a consequence, the entropy change ΔS

$$\Delta S_{\mathrm{vib}} = pR \ln(\mathrm{A}R_{\mathrm{p}}) \qquad \text{with } \mathrm{A}R_{\mathrm{p}} = 1/p\sum_{i=1}^{p} R_i \qquad (6)$$

changes from negative to positive values for p around 20.

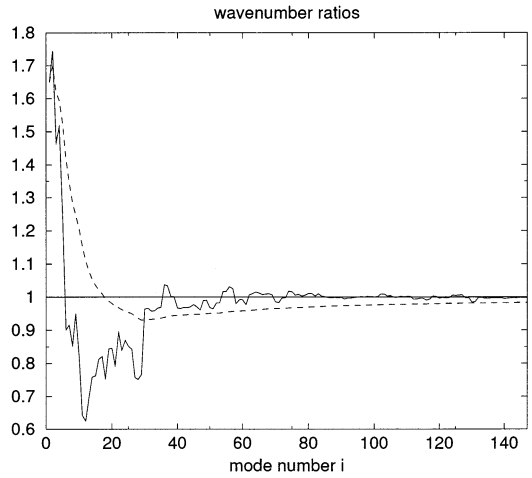

Figure 7. $(R_i)^{-1} = \tilde{\nu}_{i(\mathrm{HS})}/\tilde{\nu}_{i(\mathrm{LS})}$ of the wavenumbers of the corresponding normal modes in the HS and LS complexes. Additionally, the average ratio $\mathrm{A}(R_i)^{-1}$ (- - -) of all modes up to $\tilde{\nu}_i$ is shown (see eq 6).

The average ratio of the 50 lowest-wavenumber modes ($\tilde{\nu} \leq 571$ cm^{-1}) is only about 1.05. By inserting this number into the above approximation (eq 5), we get a similar result to Bousseksou et al.'s:

$$\Delta S_{\mathrm{vib}} = (50)(8.31) \ln 1.05 = 20.27 \text{ (J/(mol K))}$$

In view of the actual course of the average wavenumber with the number of considered modes (Figure 7), this agreement appears to be accidental.

5. Summary and Conclusion

DFT calculations employing the BP86 functional predict for the $Fe(phen)_2(NCS)_2$ complex with a cisoid arrangement of the NCS ligands a reduction in symmetry from C_2 to C_1 upon a transition from the low-spin to the high-spin state of the central iron atom. The differences between the structural parameters of the calculated isolated complex and the X-ray data suggest that crystal packing forces influence the geometry in the solid state. They are assumed to provide the necessary interaction between the individual complexes that leads to the sharp low-spin−high-spin transition. The quantum chemical calculations for the isolated complex predict correctly, nevertheless, the structural changes associated with this spin transition.

The calculated normal modes in general correlate well with the experimental IR and Raman spectra, thereby justifying the attempt to determine the entropy change associated with the molecular vibrations on the basis of the theoretical spectrum. The effect of intermolecular interaction manifests itself in a pronounced shift of the bands associated with NCS stretching. The latter is modeled by including two pyridins as a substitute for the phenanthroline ligand of the complex in the neighboring unit cell.

The estimation of the vibration-correlated entropy change yields $\Delta S_{\mathrm{vib}} \approx 19.5$ J/(mol K) independently of whether the calculation is performed via the exact partition function of all of the calculated harmonic modes or via the low-frequency approximation employed earlier by Bousseksou et al.[9] Consequently, only about 40% of the experimentally determined total entropy change of $\Delta S = 49$ J/(mol K) should originate from changes in intramolecular normal-mode frequencies. Since the change in the spin distribution contributes only about $\Delta S_{\mathrm{el}} = 14$ J/(mol K), the remainder must originate from intermolecular contributions (e.g., changes in the phonon spectrum). The latter

conclusion is in accord with the findings of Paulsen et al., who employed nuclear inelastic scattering to [Fe(tptMetame)]-$(ClO_4)_2$.[17] These authors show that the major contribution to the entropy change ΔS arises from the iron−ligand bond-stretching vibrations, but in addition, the optical phonons (and only these) should give rise to a significant entropy decrease upon the HS−LS transition.

Acknowledgment. We thank Dr. F. Renz (Universität Mainz) for many stimulating discussions and for donating a sample of $Fe(phen)_2(NCS)_2$. Financial support by the Deutsche Forschungsgemeinschaft (SFB 583) and Fonds der Chemischen Industrie is also gratefully acknowledged.

References and Notes

(1) Cambi, L.; Cagnasso, A. *Atti Accad. Naz. Lincei* **1931**, *13*, 809.
(2) Cambi, L.; Szego, L. *Ber. Dtsch. Chem. Ges*. **1931**, *64*, 259.
(3) Gütlich, P.; Hauser, A.; Spiering, H. *Angew. Chem.* **1994**, *106*, 2109.
(4) Martin, R. L.; White, A. H. *Transition Met. Chem. (NY)* **1968**, *4*, 113.
(5) König, E. *Struct. Bonding (Berlin)* **1991**, *76*, 51.
(6) Gütlich, P.; Link, R.; Trautwein, A. X. *Mössbauer Spectroscopy and Transition Metal Chemistry;* Springer: Berlin, 1978.
(7) Sorai, M.; Seki, S. *J. Phys. Chem. Solids* **1974**, *35*, 355.
(8) Takemoto, J. H.; Streusand, B.; Hutelimson, B. *Spectrochem. Acta, Part* A **1974**, *30*, 827.
(9) Bousseksou, A.; McGarvey, J. J.; Varret, F.; Real, J. A.; Tuchagues, J.-P.; Dennis, A. C.; Boillot, M. L. *Chem. Phys. Lett.* **2000**, *318*, 409.
(10) Gallois, B.; Real, J.-A.; Hauw, C.; Zarembowitch, J. *Inorg. Chem*. **1990**, *29*, 1152.
(11) Bousseksou, A.; Constant-Machado, H.; Varret, F. *J. Phys. I* **1995**, *5*, 7470.
(12) Spiering, H.; Meissner, E.; Koppen, H.; Müller, E. W.; Gütlich, P. *Chem. Phys*. **1982**, *68*, 65.
(13) Boinnard, D.; Bousseksou, A.; Dwoskin, A.; Savariault, J.-M.; Varret, F.; Tuchagues, J.-P. *Inorg. Chem*. **1994**, *33*, 271.
(14) Matouzenko, G.; Bousseksou, A.; Lecocq, S.; Van Kouingsbruggen, P. J.; Perrin, M.; Kahn, O.; Collet, A. *Inorg. Chem*. **1997**, *36*, 5869.
(15) Takemoto, J. H.; Hutchinson, B. *Inorg. Chem*. **1973**, *12*, 705.
(16) Paulsen, H.; Winkler, H.; Trautwein, A. X.; Grünsteudel, H.; Rusanov, V.; Toftlund, H. *Phys. Rev. B* **1999**, *59*, 975.
(17) Paulsen, H.; Benda, R.; Herta, C.; Schünemann, V.; Chumakov, A. I.; Duelund, L.; Winkler, H.; Toftlund, H.; Trautwein, A. X. *Phys. Rev. Lett*. **2001**, *86*, 1351.
(18) Madeja, K.; Wilke, W.; Schmidt, S. *Z. Anorg. Allg. Chem.* **1966**, *346*, 306.
(19) Ahlrichs, R.; Bär, M.; Häser, M.; Horn, C.; Kölmel, C. *Chem. Phys. Lett.* **1989**, *162*, 165.
(20) Becke, A. D. *Phys. Rev. A* **1988**, *38*, 3098.
(21) Perdew, J. P. *Phys. Rev. B* **1986**, *33*, 8822.
(22) Eichkorn, K.; Treutler, O.; Öhm, H.; Häser, M.; Ahlrichs, R. *Chem. Phys. Lett.* **1995**, *240*, 283.
(23) Eichkorn, K.; Weigend, F.; Treutler, O.; Ahlrichs, R. *Theor. Chem. Acc*. **1997**, *97*, 119.
(24) Schäfer, A.; Huber, C.; Ahlrichs, R. *J. Chem. Phys.* **1994**, *100*, 5829.
(25) Kind, C.; Reiher, M.; Neugebauer, J.; Hess, B. A. *SNF;* University of Erlangen-Nürnberg: Nürnberg, Germany, 1999−2001.
(26) Neugebauer, J.; Reiher, M.; Kind, C.; Hess, B. A. *J. Comp. Chem.* **2002**, *23*, 895.
(27) Reiher, M. *Inorg. Chem.*, in press.
(28) Reiher, M.; Neugebauer, J.; Hess, B. A. *Z. Phys. Chem. (München)*, in press.
(29) Sellmann, D.; Gottschalk-Gaudig, T.; Häussinger, D.; Heinemann, F. W.; Hess, B. A. *Chem.—Eur. J.* **2001**, *7*, 2099.
(30) Salomon, O.; Reiher, M.; Hess, B. A. *J. Chem. Phys.* **2002**, *117*, 4729.
(31) Reiher, M.; Salomon, O.; Hess, B. A. *Theor. Chem. Acc.* **2001**, *107*, 48.
(32) Reiher, M.; Brehm, G.; Schneider, S. *Chem. Phys.*, submitted for publication.